SLAC-PUB-12041
August 2006

Search for Oxygen Emission from Warm-Hot Intergalactic Medium around A2218 with *Suzaku*

Yoh TAKEI[1], Takaya OHASHI[2], J. Patrick HENRY[3], Kazuhisa MITSUDA[1], Ryuichi FUJIMOTO[1], Takayuki TAMURA[1], Noriko Y. YAMASAKI[1], Kiyoshi HAYASHIDA[4], Noriaki TAWA[4], Kyoko MATSUSHITA[5], Mark W. BAUTZ[6], John P. HUGHES[7], Grzegorz M. MADEJSKI[8], Richard L. KELLEY[9], Keith A. ARNAUD[9]

[1] *Institute of Space and Astronautical Science, Japan Aerospace Exploration Agency, 3-1-1 Yoshinodai, Sagamihara, Kanagawa 229-8510*
takei@astro.isas.jaxa.jp

[2] *Department of Physics, Tokyo Metropolitan University, 1-1 Minami-Osawa, Hachioji, Tokyo 192-0397*

[3] *Institute for Astronomy, University of Hawai'i, 2680 Woodlawn Drive, Honolulu, HI 96822, USA*

[4] *Department of Astrophysics, Faculty of Science, Osaka University, Toyonaka 560-0043*

[5] *Department of Physics, Tokyo University of Science, 1-3 Kagurazaka, Shinjuku, Tokyo 162-8601*

[6] *Kavli Institute for Astrophysics and Space Research, Massachusetts Institute of Technology, 70 Vassar Street, Building 37, Cambridge, MA 02139, USA*

[7] *Department of Physics and Astronomy, Rutgers University, Piscataway, NJ 08854-8019, USA*

[8] *Stanford Linear Accelerator Center, 2575 Sand Hill Road, Menlo Park, CA 94025, USA*

[9] *NASA Goddard Space Flight Center, Code 662, Greenbelt, MD 20771, USA*

(Received 2006 July 19; accepted)

Abstract

We searched for redshifted O emission lines from the possible warm-hot intergalactic medium (WHIM) surrounding the cluster of galaxies A2218 at $z = 0.1756$ using the XIS instrument on *Suzaku*. This cluster is thought to have an elongated structure along the line of sight based on previous studies. We studied systematic uncertainties in the spectrum of the Galactic emission and in the soft X-ray response of the detectors due to the contamination building up on the XIS filters. We detected no significant redshifted O lines, and set a tight constraint on the intensity with upper limits for the surface brightness of O VII and O VIII lines of 1.1×10^{-7} and 3.0×10^{-7} photons cm^{-2} s^{-1} arcmin^{-2}, respectively. These upper limits are significantly lower than the previously reported fluxes from the WHIM around other clusters of galaxies. We also discuss the prospect for the detection of the WHIM lines with *Suzaku* XIS in the future.

Key words: cosmology: large-scale structure — galaxies: clusters: individual (A2218) — intergalactic medium — X-rays: diffuse background

1. Introduction

Based on several N-body simulations of cosmological large-scale structure formation (e.g., Cen & Ostriker, 1999; Davé et al., 2001; Chen et al., 2003), a significant (30–50%) fraction of baryons is thought to reside in the form of gas in a 'warm-hot' phase ($T = 10^{5-7}$ K), which is hard to detect with the instruments currently in operation. This warm-hot gas, whose density is 10^{-6}–10^{-4} cm^{-3}, is called the warm-hot intergalactic medium (WHIM). The firm detection of the WHIM is important because it is the most promising candidate for the "missing baryons"; i.e., it is thought to explain the discrepancy between the baryon density observed in the local universe (Fukugita et al., 1998) and that in the distant universe (Rauch et al., 1997) or that calculated from the observed fluctuations of the cosmic microwave background (Spergel et al., 2003).

The WHIM may be detected via emission or absorption lines from highly ionized elements in UV or X-ray spectra. Given the relative elemental abundances, — on the order of 0.1 to 0.3 of Solar — oxygen is the most promising element to provide detectable transitions at the expected temperatures. Over 40 systems show O VI absorption features, based on observations from *FUSE* and *HST* (e.g. Danforth & Shull, 2005). However, their analysis shows that the baryon density in the temperature range $T = 10^{5-6}$ K is about an order of magnitude lower than the expected WHIM level. Therefore, most of the missing baryons seem to reside in a hotter phase at $T = 10^{6-7}$ K, which can be probed with X-rays. There is only one sightline with a likely detection of the WHIM via O VII or O VIII absorption lines so far (Nicastro et al., 2005). Their results suggest that most of the missing baryons can be explained by the absorbing clouds inferred from their data. However, recent work by Rasmussen et al. (2006) and Kaastra et al. (2006) showed that the detection with the Chandra LETGS by Nicastro et al. (2005) was not consistent with RGS observations of

Submitted to Astronomical Society, Japan
Work supported in part by DOE Contract No. DE-AC02-76SF00515

the same sight line. Thus, the existence of the WHIM in the hotter phase is not yet confirmed.

Several possible detections of WHIM emission have been reported. Kaastra et al. (2003) and Kaastra (2004) report the detection of redshifted O VII and O VIII emission lines as well as soft X-ray ($E < 0.5$ keV) excesses in the spectra of 7 clusters of galaxies out of 21 measured systems. Finoguenov et al. (2003) also reported detection of O VII and O VIII emission lines in the outskirts of the Coma cluster. Fujimoto et al. (2004) and Takei et al. (2006) report not only emission lines in the spectrum of cluster outskirts but also absorption lines in the spectrum of a quasar behind the clusters, although the significance of the absorption measurement is not high ($< 3\sigma$). Fujimoto et al. (2004) observed O VIII features in the Virgo cluster, while Takei et al. (2006) detected Ne IX in the Coma cluster. They estimated the path length of absorbing/emitting medium assuming that the absorber and the emitter are the same cloud, and concluded that the length scale of the medium exceeds the virial scale of the clusters. There are counterarguments against the discovery of O VII or O VIII emission lines associated with clusters. For example, Bonamente et al. (2005) and Bregman & Lloyd-Davies (2006) concluded that some of the emission lines observed by Kaastra et al. (2003) are likely due to field-to-field variation of the soft X-ray background or Galactic emission. Such controversies occurred because the CCD instruments cannot clearly distinguish O lines emitted by the gas associated with clusters of moderate redshift ($z \lesssim 0.05$) from those of Galactic origin. These arguments suggest the importance of careful target selection and accurate measurement of background level. Note that the observations of redshifted emission lines also give important clues to solve another mystery "cluster soft excess", the excess emission in $E < 0.3$ keV, reported since the 1990s in the extreme ultraviolet and the X-ray bands from *EUVE* and *ROSAT* (e.g., Lieu et al., 1996a; Lieu et al., 1996b; Mittaz et al., 1998; Bowyer et al., 2004). Thus, the study of X-ray emission in cluster outskirts brings us important information about the cluster system itself and its environment.

Since there are only a few reports of possible emission lines from the WHIM, further sensitive study of other systems is desirable. In this paper, we report our observation of A2218 with the XIS (Koyama et al. 2006) onboard *Suzaku* (Mitsuda et al. 2006). A2218 is a well-known cluster because of its strong gravitational lensing arcs. Its redshift is 0.1756 (Struble & Rood, 1999), where one arcminute corresponds to 179 kpc with the cosmology we have adopted. The cluster is thought to be still in a dynamically young state — X-ray analysis suggests that the cluster core is not in hydrostatic equilibrium due to an ongoing or recent merger (Pratt et al., 2005; Machacek et al., 2002) in the line-of-sight direction. The distribution of galaxy velocities based on the optical study of Girardi et al. (1997) indicates substructure in the line of sight, and Smith et al. (2005) studied the mass structure in detail and have concluded that A2218 is unrelaxed. The dynamics of the cluster is considered to cause the discrepancy between the mass estimated from gravitational lensing and that determined from X-ray observations; gravitational lensing indicates ~ 3 times higher mass than X-ray estimation for the central ($\sim 20''$) region. These observations indicate an elongated structure in the line-of-sight direction and suggests existence of a large-scale filament in this direction. If this is the case, we would expect a high surface brightness of the WHIM emission. The fairly large redshift of A2218 would also help us observe a significant energy shift of emission lines with the XIS instrument. Thus, A2218 seems to be one of the most suitable targets to search for the WHIM emission from Suzaku.

We assume a Hubble constant of 70 km s^{-1} Mpc^{-1} or $h_{70} = 1$ and $\Omega_{\rm m} = 0.3$, $\Omega_\Lambda = 0.7$. The solar metal abundances used in this paper are given by Anders & Grevesse (1989). Unless otherwise stated, errors in the figures are at the 68 % confidence level and at the 90 % confidence level in the text and tables.

2. Observations

We carried out four observations to study the warm-hot gas in the A2218 vicinity with the XIS instrument onboard *Suzaku*: two on the cluster and two in offset regions whose locations are different from each other. The offset observations were performed to measure the foreground Galactic contribution, which can produce a large ambiguity in the study of soft emission around clusters. Fig. 1 is a map of the *ROSAT* R4 band after removing bright point sources (Snowden et al., 1997). This energy band is sensitive to O VII and O VIII emission lines, which are strong in the Galactic emission, and hence is suitable to study their fluctuations.

We examined the *ROSAT* map (Fig. 1) and selected the location of offset pointings so that the Galactic emission level is similar to that in the vicinity of A2218. Also, the distance from A2218 is large ($\gtrsim 1^\circ$ or 10.7 Mpc at the A2218 redshift), so the data from the offset regions should be free from the putative large-scale filament around A2218. The observed locations are shown in Fig. 1 and Table 1, as well as the position of A2218. Hereafter we call the four observations A2218-1, A2218-2, Offset-A, and Offset-B, respectively. A2218-1 and Offset-A were observed in early October, 2005, and the others in late October. The observation sequence numbers and dates are summarized in Table 2.

The XIS is an X-ray CCD camera, which consists of three front-illuminated (FI) sensors and one back-illuminated (BI) sensor. The camera covers the 0.2–12 keV energy band with an energy resolution of 130 eV at 5.9 keV and 40 eV at 0.5 keV. Its field of view is a square of $18' \times 18'$. The BI and FI sensors have different advantages: the former has higher quantum efficiency in the soft energy band, while the latter shows a lower internal background level. An important characteristic of the XIS is the absence of a large low-energy tail in the pulse-height distribution

function, even in the very soft energy ($E \lesssim 0.5$ keV) band. Those characteristics give the XIS an excellent capability to study the low-energy emission lines, such as from the WHIM. After the launch of *Suzaku*, a time and position dependent contamination of the XIS optical blocking filter (OBF) was found. The source is probably outgassing from the satellite. The level of contamination increases with time and is different from sensor to sensor. The time and position dependence of the contamination thickness has been empirically modeled by the XIS team. At the time of our observations, the effective area at 0.5 keV was on average 25% lower than that of the pre-launch calibration. See Koyama et al. (2006) for a fuller description of the instrument. The two observations of A2218 were 25 days apart, and the count rates at 0.5 keV were different by 9% and 13% for the BI and the combined FI sensors, respectively. This is consistent with the expected drop of 8% for both sensors within statistical errors.

The XIS instrument was operated in normal mode in all the observations presented in this paper. We used event files of version 0.7 products[1]. Events of 3×3 and 5×5 observation modes were combined. The first few kiloseconds of each observation, when the pointing direction had not yet stabilized, were excluded. The resulting image of A2218 in the 1.0–4.0 keV energy band is shown in Fig. 2. Data from the two observations and the four CCDs are combined. The white circles indicate the region where we extracted the spectra. The radii are $3'$ and $8'$ from the cluster center, corresponding to 540 and 1430 kpc at the source, respectively.

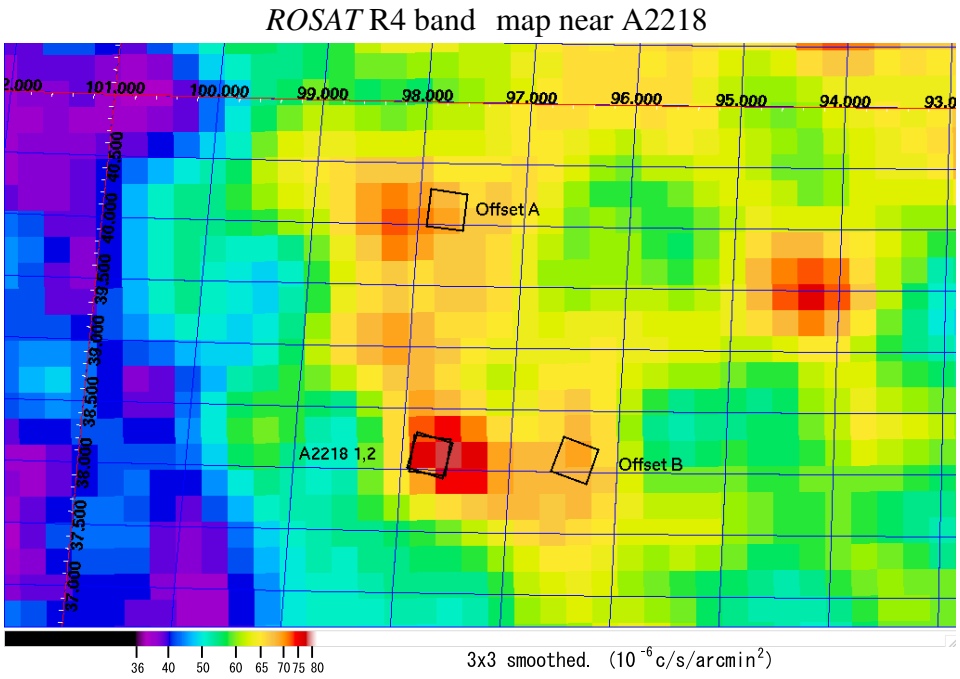

Fig. 1. *ROSAT* R4 band image around A2218 (Snowden et al., 1997) in Galactic coordinates. The field of view of XIS in the four observations are indicated by black squares. Most of the emission in this band is O VII and O VIII line.

Table 1. Position of the A2218 and offset pointing

	(RA, Dec)	(l, b)
A2218	($16^h35^m54^s$, $66°13'00''$)	(97.7449, 38.1235)
Offset-A	($16^h17^m48^s$, $65°27'36''$)	(97.7423, 40.1239)
Offset-B	($16^h39^m31^s$, $66°13'31''$)	(96.4000, 38.1002)

[1] Version 0 processing is an internal processing applied to the Suzaku data obtained during the SWG phase. Aspect correction and fine tuning of the event time tagging are skipped in this version. Times when the elevations from the bright and dark Earth are $> 20°$ and $> 5°$ are excised in standard data processing.

Table 2. *Suzaku* observations of A2218 and offset pointing

	Sequence number	Date	Exposure after processing	Net exposure using all COR	Net exposure using COR> 8 Gev c^{-1}
A2218-1	100030010	2005-10-01–2005-10-02	46.4 ks	44.9 ks	38.2 ks
A2218-2	800019010	2005-10-26–2005-10-27	32.8 ks	32.3 ks	28.8 ks
Offset-A	100030020	2005-10-02–2005-10-03	44.6 ks	44.6 ks	39.0 ks
Offset-B	800020010	2005-10-27–2005-10-27	15.0 ks	15.0 ks	12.0 ks

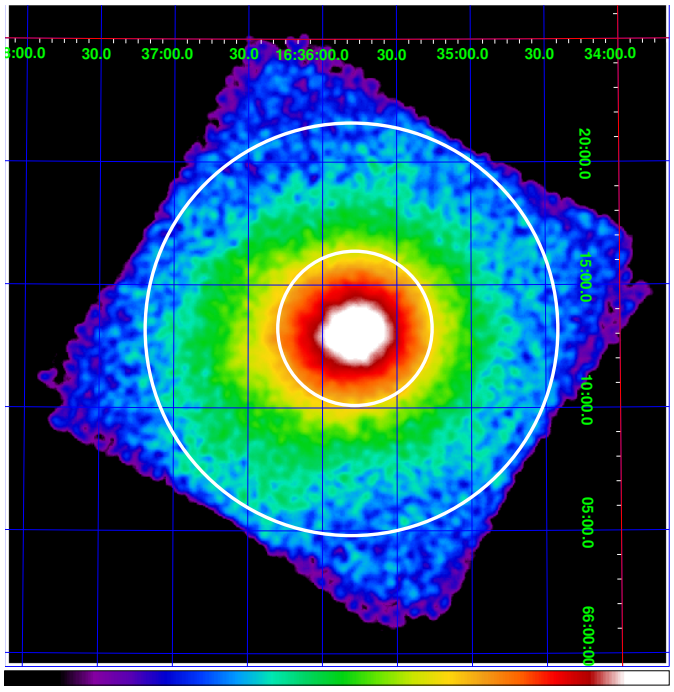

Fig. 2. Image of A2218 in the 1.0–4.0 keV band observed with the XIS. The events of the two observations obtained by four CCDs were summed. The spectra were extracted from the annulus between the two white circles. Vignetting effects were not taken into account for this image and background events were not subtracted. The grid indicates the coordinates in J2000.0.

3. Spectral analysis

3.1. Analysis method

We removed flickering CCD pixels, which cause a large noise component below 0.5 keV. We also excluded apparent point sources that were found in the Offset-A image. Although the fluxes of these point sources were lower than the detection limit for the A2218 image, we removed them because we are interested in the upper limits of the soft excess emission. The spectra were then extracted in the annular region between $3'$ and $8'$ from the cluster center using XSELECT distributed in HEASOFT 6.0.4. We define the cluster center as (DETX, DETY) = (499, 530) in detector coordinates for all observations and all sensors. Note that the boresight of all XIS sensors coincide within $20''$. We have chosen the inner radius to be $3'$ in order to exclude the bright central region, in which the strong emission of the hot ICM hampers the study of warm-hot emission. We also excluded the region outside of $8'$ because the position dependence of the contamination on the OBF is not well known there. Although the XIS sensors are always illuminated by ^{55}Fe calibration sources at the field edge, we did not remove these regions in the present analysis.

To estimate and subtract the internal background, we also extracted spectra from night Earth observations distributed by the XIS team. It is known that the variation of the internal background spectrum is well correlated with the cut-off rigidity (COR) at the position of the satellite; the smaller the COR value is, the larger the background level becomes. To estimate accurately the internal background level, we collected events when the detector was looking at the dark Earth (night Earth events) and sorted them by COR. We extracted the spectrum for each 1 GeV c^{-1} interval of COR, and then added them weighted by exposure time for the respective COR range in the actual observation. This process gives different night Earth spectra for the four observations, since the detailed distribution of COR was different among the observations. The background spectra were extracted from the same region in detector

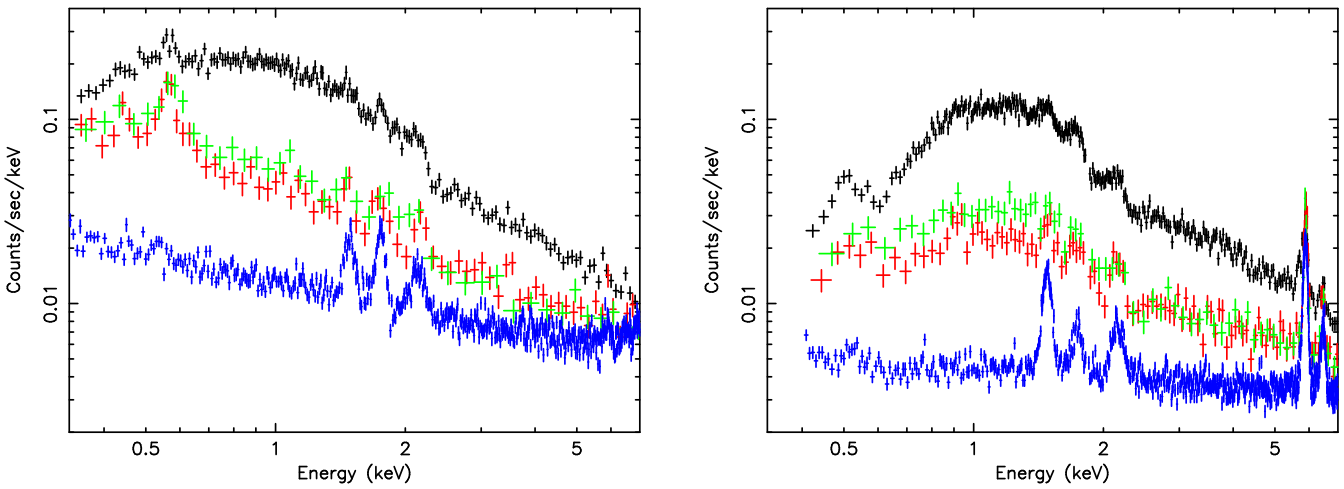

Fig. 3. Spectra of A2218 taken with the (left) BI and (right) FI chips, where three FI spectra were averaged. Black, red, green and blue points show A2218, Offset-A, Offset-B, night earth spectra, respectively. The strong peaks at 5.9 keV and 6.5 keV in the right panel are due to the calibration sources.

coordinates as the corresponding observation in order to avoid possible systematic effects due to positional variation of the detector background.

We used response matrix files (RMFs) ae_xi[0123]_20060213(c).rmf distributed by the XIS team for spectral fitting. On the other hand, we generated the ancillary response files (ARFs) with the arf builder 'xissimarfgen', which is based on ray-tracing (Ishisaki et al. 2006). The change of the effective area with time in the soft X-ray energy range, due to the increase of OBF contamination, was taken into account by the following method. The ARFs were created separately for each observation, according to the observation date. We used the ae_xi[0123]_contami_20060525.fits contamination tables to model the composition and position dependence of the contaminant, in which the C/O ratio of contaminant was assumed to be 6. Note that the effective area for diffuse sources depends on the sky distribution of the flux, because the quantum efficiency varies with the detector position due to vignetting and contamination thickness. We adopted the Suzaku XIS image (1.0–4.0 keV) of A2218 for the incident flux distribution, in which the two observations by the four sensors were all summed (see Fig. 2). We assumed a uniform flux distribution for the offset pointings.

In the analysis shown below, the spectra and ARFs for A2218-1 and A2218-2 were added using the ftools mathpha and addarf, respectively. Further, the spectra and response (RMFs and ARFs) of the three FI sensors were combined using ftools mathpha and marfrmf, respectively. We confirmed that consistent results were obtained with this treatment within the statistical error. We fitted spectra of the offset observations in the 0.35 keV $< E <$ 5.0 keV energy range for the BI and 0.40 keV $< E <$ 5.0 keV except the energy of anomalous response at the Si K-edge, 1.825–1.840 keV, for the FI. When we fitted the spectra of A2218, the energy range was extended up to 7.0 keV in order to cover the Fe-K lines. We excluded 5.85–5.95 keV and 6.45–6.55 keV, because the slight difference in intensity of Mn K emission lines from the ^{55}Fe calibration sources between A2218 observations and night Earth observations causes relatively large residuals. The spectra of A2218 (black), Offset-A (red), and Offset-B (green), as well as the night Earth spectra (blue) are shown in Fig. 3. Left and right panels are for BI and FI spectra, respectively. The difference in the detector area due to point-source exclusion was corrected in the figure for illustrative purposes. We mainly performed simultaneous fits for the two spectra obtained by the BI and the combined FI sensors. However, it was also confirmed that the spectrum with the BI sensor only gave consistent results. This indicates that the uncertainty in the FI response around 0.5 keV is not crucial compared with the statistical errors in the BI spectrum.

Evaluation of the systematic uncertainties is crucial in constraining the emission from the WHIM. Firstly, the emission is in the soft X-ray region where the XIS has various systematic uncertainties, so we have to look into many possible effects. Secondly, the observation was carried out only three months after the launch of *Suzaku*, and time variation of the detector response needs to be carefully considered.

The first uncertainty is the detector response. The largest systematic uncertainty in the detector response is the thickness of contaminant on the OBF of the XIS. In the 0.4–0.6 keV band, most of the photons we observe are thermal emission from the ICM. If we underestimate the contaminant thickness, the flux from the ICM would be overestimated in $E \lesssim 1$ keV, because the temperature and abundance are strongly constrained by the data in the higher energy range $E \gtrsim 1$ keV. This naturally leads to an underestimation of the soft-excess flux. Therefore, we also considered a *thicker* contaminant model at the upper limit of the uncertainty range. We generated ARFs with 20% thicker contaminant using xissimarfgen assuming the observation occurred seventeen days later than it actually did. This 20% increase,

which exceeds the uncertainty quoted by the XIS team ($\sim 10\%$; Koyama et al. 2006), is a reasonable value, given the additional uncertainties in the response to diffuse emission and in early observations. The energy resolution of the XIS worsens with time. At the time of our observations, the energy resolution had degraded by ~ 20 eV (FWHM) at 5.9 keV (from 130 eV to 150 eV). This effect was investigated by smoothing the response with a Gaussian. Since we have no information about the degradation at ~ 0.5 keV, we tried Gaussians with sigmas of 5 eV, 10 eV, 15 eV, 20 eV, 30 eV and 35 eV. With this smoothing, the spectral resolution at $\sim$0.5 keV increases from 40 eV to 42 eV, 46 eV, 53 eV, 62 eV, 81 eV and 91 eV, respectively. The results are presented later. The internal background of the XIS is quite stable, and there were no "background flares" during our observations. However, when COR is low (COR$\lesssim 6$ GeV c^{-1}), the internal background level becomes comparable to the X-ray background in the $E > 3$ keV range. Therefore, we also extracted spectra with the condition COR > 8 GeV c^{-1} to examine this systematic effect.

Another uncertainty is the spatial variation of the Galactic emission. The *ROSAT* R4 map shows $\sim 10\%$ variations among the A2218, Offset-A and Offset-B fields. The purpose of the two offset observations (Offset-A and Offset-B) was to look at the spectral variation in the Galactic emission and to include it in the analysis. Besides the inclusion of this variation, we also extended our upper limit for the soft excess by assuming 10% fainter Galactic emission.

3.2. Offset pointings

Before the analysis of the A2218 spectrum, we analyzed data from the offset pointings to estimate the spectrum of the Galactic emission. The diffuse X-ray background at high Galactic latitude can be divided into three components: i.e. the local hot bubble (LHB), the Milky Way halo (MWH) and the extragalactic power-law (CXB) components (Snowden et al., 1998). Typical temperatures are about 0.1 keV for the LHB and 0.2–0.3 keV for the MWH, while the CXB spectrum has a photon index of 1.4. The LHB is thought to surround the solar system with a ~ 100 pc scale, and hence it has no Galactic absorption. The CXB component is extragalactic and known to be uniform over the entire sky. In contrast, the level of LHB and MWH components vary from position to position. Lumb et al. (2002) reported that the mean deviation of the 0.2–1.0 keV intensity is $\sim 35\%$ from field to field.

Our purpose here is to constrain the spectra of the two Galactic components so as to obtain reliable background data for the estimation of the warm emission around A2218. Spectra for an annular region with $r = 3' - 8'$ were produced for the Offset-A and Offset-B data. XSPEC v11.3.2r was used in the spectral analysis. The spectra, from which non X-ray background was subtracted, were fitted with a model for the sum of LHB, MWH and CXB. CXB and MWH components were absorbed by Galactic absorption characterized by $N_{\rm H} = 3.24 \times 10^{20}$ cm^{-2} (Dickey & Lockman, 1990). The collisionally ionized thermal plasma model APEC was used in XSPEC to fit the LHB and MWH spectra, with abundance and redshift fixed to 1 solar and 0, respectively. The photon index of the power-law CXB model and the temperature of the LHB were fixed to 1.4 and 0.08 keV, respectively. The normalizations of the FI and BI sensors were allowed to take different values.

The best-fit parameters and the model curves are shown in Table 3 and Fig. 4. In Table 3, parameters except for the FI/BI ratio are for the BI spectra. Acceptable fits were obtained for the two spectra and the parameters of the Galactic emission were well constrained. The normalization of the CXB component agrees with previous reports (Kushino et al., 2002). The flux in the 0.5–2.0 keV band of Offset-A and Offset-B observation differs by $\sim 10\%$. Not only the flux, but also the shape of the best-fit model is different between the two observations, which is either due to the poor statistics of the Offset-B observation or real variations in the Galactic emission.

Table 3. Best-fit parameters of offset pointings

Parameter	Offset-A	Offset-B
LHB kT (keV)	0.08 (fixed)	0.08 (fixed)
LHB Normalization[a]	$3.2 \pm 1.0 \times 10^{-6}$	$6.2^{+0.7}_{-1.7} \times 10^{-6}$
MWH kT (keV)	$0.158^{+0.028}_{-0.018}$	$0.248^{+0.033}_{-0.031}$
MWH Normalization[a]	$6.7^{+3.3}_{-2.5} \times 10^{-7}$	$5.0^{+1.5}_{-1.0} \times 10^{-7}$
CXB Photon index	1.4 (fixed)	1.4 (fixed)
CXB Normalization[b]	$8.5 \pm 0.5 \times 10^{-7}$	$8.5 \pm 0.7 \times 10^{-7}$
FI/BI ratio	0.84 ± 0.05	1.04 ± 0.09
χ^2/dof	154.03/149	100.45/93

[a] $\int n_{\rm e} n_{\rm H}\ dV/4\pi(D_{\rm A}(1+z))^2$ per solid angle in units of 10^{14} cm^{-5} arcmin^{-2}, where $n_{\rm e}$ is the electron density, $n_{\rm H}$ the hydrogen density, and $D_{\rm A}$ the angular size distance.
[b] In units of photons cm^{-2} s^{-1} keV^{-1} arcmin^{-2} at 1 keV

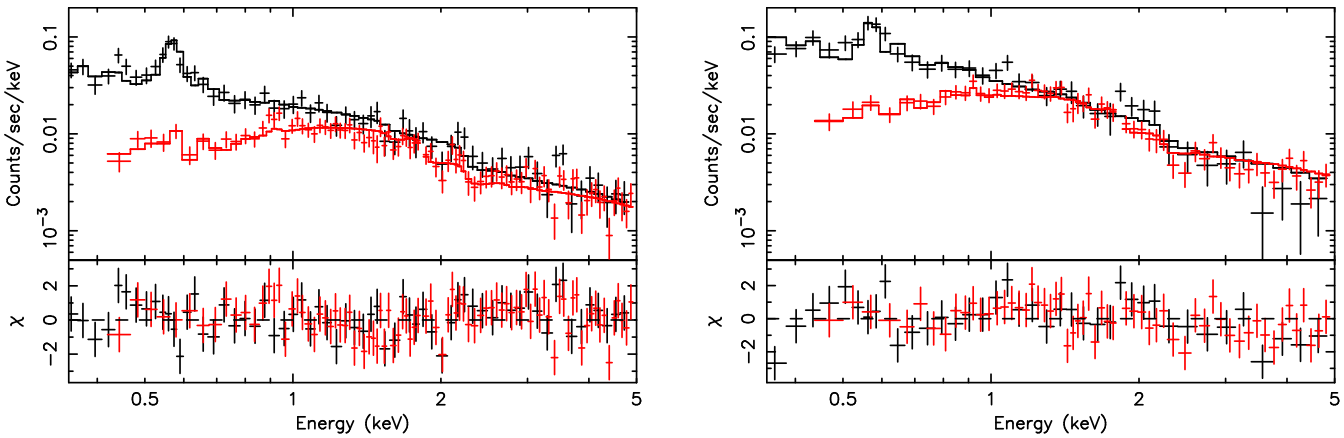

Fig. 4. Spectra and best-fit models, and residuals of offset observations. (left) Offset-A, (right) Offset-B. Black and red represents BI and FI sensors.

3.3. A2218

3.3.1. Single temperature model

The A2218 spectrum for the radial region of $3' - 8'$ was analyzed here. The summed FI and the BI spectra were fitted simultaneously. Before testing the warm emission in the model, we first fitted with a model only including the thin thermal plasma (ICM) and the background emission determined from the offset-region spectra. We tried two models for the background: namely, the best-fit models for the BI spectra determined from the Offset-A and Offset-B observations. We fixed all the parameters for the background spectrum consisting of LHB, MWH and CXB at the best-fit values. The redshift of the hot ICM was fixed at 0.1756. We allowed the FI/BI normalization to be free again. The results of the fit are summarized in Table 4 and in Fig. 5. The different background (Offset-A or B) gives an ICM temperature differing by about 10%, while similar metal abundance values were obtained in the two cases. The temperature and abundance are generally consistent with previously determined values; *XMM-Newton* spectra indicates $kT \sim 5$ keV in $3' - 5'$ and $Z = 0.13 \pm 0.04$ solar in the central $5'.1$ region (Pratt et al., 2005), while *Chandra* estimated kT to be 6.9 ± 0.5 and Z to be 0.20 ± 0.13 in the central $5'.1$ region (Machacek et al., 2002). The detailed analysis of the temperature and abundance of the ICM will be reported elsewhere.

The spectra were well fitted with this simple model, suggesting that no obvious soft excess is present. The residual of the spectral fit should indicate a feature, such as that caused by redshifted oxygen lines, if warm emission indeed gives a significant contribution. Both panels in Fig. 5 suggest some features around 0.57 keV and 0.68 keV: the former is a positive residual, while the latter negative. Both features are near the strong Galactic O emission lines: O VII at 574 eV and O VIII at 654 eV, and not identical to those of redshifted O lines at the redshift of A2218. Their levels are less than that of Galactic emission by a factor of 3–10. Hence, they may originate in the fluctuation or incomplete modeling of Galactic emission. Note that the O VIII line (654 eV) at the source is redshifted to 556 eV, which is close to the strong O VII line (574 eV) in the Galactic emission. Thus it is rather difficult to detect the warm gas with this line. The redshifted O VII line (574 eV shifts to 488 eV) is also close to the peak caused by the oxygen edge of the detector deadlayer and OBF, in particular for the FI sensors (see Fig. 4 of Koyama et al. 2006). These situations make the XIS sensitivity to warm gas for a source with redshift similar to that of A2218 poorer than it is at other redshifts. We will carry out a quantitative evaluation in the next section.

3.3.2. Constraint on redshifted O lines

We performed another spectral fit by adding two Gaussian emission lines to the model, in order to test for the existence of redshifted O lines. The energies of the lines were fixed to 488.22 eV and 555.99 eV, which correspond to O VII (resonance) and O VIII lines at $z = 0.1756$. Although the energy of the O VII line could be at most 10 eV lower due to the contribution of intercombination and forbidden lines, we confirmed that the results shown below are not affected by that difference in energy. The intrinsic widths were fixed to zero. The temperature and abundance of the ICM component were free parameters, while all the background parameters (for LHB, MWH and CXB) including the normalizations were fixed at the best-fit values determined with the Offset data described in § 3.3.1. The free parameters were the temperature kT, abundance Z and normalization of the ICM, the surface brightness I of redshifted O VII and O VIII lines, and FI/BI normalization ratio. We again tried the two background models, determined from the Offset-A and Offset-B observations, respectively.

The best-fit parameters and improvement in χ^2 values are shown in Table 5. The obtained surface brightness I of the lines is small and consistent with zero; the improvement in χ^2 is less than 2.71 (90% significance for 1 free

Table 4. Best-fit parameters of A2218 with single temperature model

Parameter	Offset-A Case	Offset-B Case
LHB kT (keV)	0.08 (fixed)	0.08 (fixed)
LHB Normalization[a]	3.2×10^{-6} (fixed)	6.2×10^{-6} (fixed)
MWH kT (keV)	0.158 (fixed)	0.248 (fixed)
MWH Normalization[a]	6.7×10^{-7} (fixed)	5.0×10^{-7} (fixed)
CXB Photon index	1.4 (fixed)	1.4 (fixed)
CXB Normalization[b]	8.5×10^{-7} (fixed)	8.5×10^{-7} (fixed)
ICM kT (keV)	$5.40^{+0.27}_{-0.15}$	6.00 ± 0.22
ICM Z (solar)	0.20 ± 0.04	0.21 ± 0.04
ICM z	0.1756 (fixed)	0.1756 (fixed)
ICM Normalization[a]	$2.08 \pm 0.03 \times 10^{-5}$	$2.00 \pm 0.03 \times 10^{-5}$
FI/BI ratio	0.89 ± 0.01	0.90 ± 0.01
χ^2/dof	475.21/475	520.72/475

[a] $\int n_{\rm e} n_{\rm H}\ dV/4\pi(D_{\rm A}(1+z))^2$ per solid angle in units of 10^{14} cm^{-5} arcmin^{-2}, where $n_{\rm e}$ is the electron density, $n_{\rm H}$ the hydrogen density, and $D_{\rm A}$ the angular size distance.
[b] In units of photons cm^{-2} s^{-1} keV^{-1} arcmin^{-2} at 1 keV

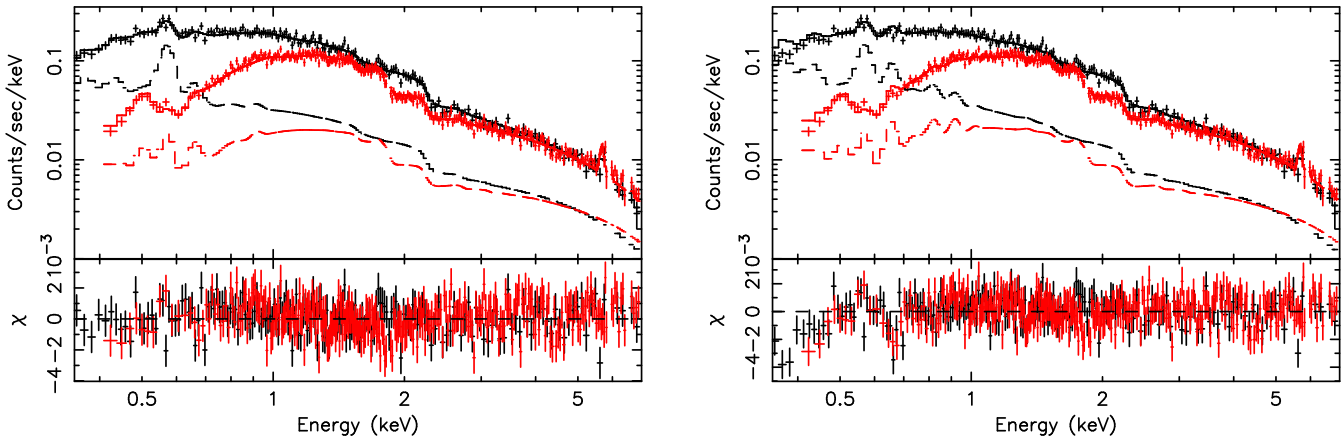

Fig. 5. Spectra fitted with the best-fit models, and residuals of A2218 observations, in which the data from the two observations were merged. Galactic components are fixed to (left) Offset-A, and (right) Offset-B models, respectively. Black and red indicate BI and FI sensors. The contribution of the Galactic emission, determined by offset observations, are also indicated by dashed lines.

parameter). We then constrained the allowed O line intensity range. The upper limits for the O VII and O VIII I were estimated from that causing an increment of the χ^2 value by 4.0 (2σ limit) over the minimum (best-fit) level. In this process, we allowed the other free parameters (i.e., the ICM temperature, abundance, normalization, and FI/BI ratio) to vary. The upper limits of the two lines were determined separately, and the values are also shown in Table 5 in parentheses. Fig. 6 shows the model with the upper-limit intensities of the O VII and O VIII lines in the upper 2 panels; the left panel is the case with the background of Offset-A, while the right panel is for Offset-B. The upper limits are shown with solid lines, while the background spectrum is shown with dashed lines. The upper limits of the two O lines are 10–20% of the background level at the center energy of each line.

It should be noted that the O VIII line is also produced by the ICM ($T \sim 5$ keV), while O VII is not. The intensity, which depends on the temperature and O abundance, is 2×10^{-8} photons cm^{-2} s^{-1} arcmin^{-2} assuming the parameters in Table 4. However, this value contains an uncertainty; while the abundance was mostly determined by the Fe K and L features in the fit, Fe and O abundances may have a different value. We estimated the upper limit of I for the redshifted O VIII line from the WHIM in the extreme case of no O in the ICM, because this situation gives the largest contribution from the WHIM. The upper limit then increased to 1.6×10^{-7} photons cm^{-2} s^{-1} arcmin^{-2} and 1.8×10^{-7} photons cm^{-2} s^{-1} arcmin^{-2} for the Offset-A and Offset-B backgrounds, respectively.

Next, we investigated how the upper limits of I change by considering the systematic uncertainties described in § 3.1. We already checked one of these uncertainties in Table 5: variation of the Galactic emission between Offset-A and Offset-B fields. The difference is $\lesssim$20%. When we used the ARFs with 20% thicker contaminant, the upper limits of the

O VII and O VIII lines increased by $\sim 130\%$ and $\sim 30\%$, respectively. These limits further increase by $\sim 15\%$ and $\sim 30\%$ for the respective lines, if we adopt 10% fainter Galactic emission. On the other hand, the upper limits do not increase when we select the data for the low background condition (COR>8 GeV c^{-1}) or when the energy resolution of the detector was artificially degraded by 5–35 eV. To summarize, the conservative upper limits are derived by assuming no O in the ICM and employing the ARFs with 20% thicker contaminant and 10% fainter Galactic model for the Offset-B observation; the values are 1.1×10^{-7} photons cm^{-2} s^{-1} arcmin^{-2} and 3.0×10^{-7} photons cm^{-2} s^{-1} arcmin^{-2} for O VII and O VIII lines, respectively. We adopt these values as the upper limits of the O line intensity around A2218, considering both statistical and systematic errors. The spectra with the model with these upper limits are shown in the lower panel of Fig. 6. Note that even after considering these systematic errors, the upper limits are still $\sim 30\%$ of the level of the Galactic emission at the same energy.

Table 5. Best-fit parameters using a model with redshifted O lines

Parameter	Offset-A Case	Offset-B Case
ICM kT (keV)	$5.41^{+0.28}_{-0.16}$	6.02 ± 0.22
ICM Z (solar)	0.20 ± 0.04	0.21 ± 0.04
ICM z	0.1756 (fixed)	0.1756 (fixed)
ICM Normalization[a]	$2.08 \pm 0.03 \times 10^{-5}$	$2.00 \pm 0.03 \times 10^{-5}$
O VII E (eV)	488.22 (fixed)	488.22 (fixed)
O VII I[b] [c]	0 ($< 3.7 \times 10^{-8}$)	0 ($< 3.9 \times 10^{-8}$)
O VIII E (eV)	555.99 (fixed)	555.99 (fixed)
O VIII I[b] [c]	4.0 (< 13.4) $\times 10^{-8}$	6.8 (< 15.8) $\times 10^{-8}$
FI/BI ratio	0.89 ± 0.01	0.90 ± 0.01
$\Delta\chi^2/\Delta dof$	0.78/2	2.25/2

[a] $\int n_{\rm e} n_{\rm H}\ dV/4\pi(D_{\rm A}(1+z))^2$ per solid angle in units of 10^{14} cm^{-5} arcmin^{-2}, where $n_{\rm e}$ is the electron density, $n_{\rm H}$ the hydrogen density, and $D_{\rm A}$ the angular size distance.
[b] In units of photons cm^{-2} s^{-1} arcmin^{-2}
[c] Upper limits are quoted in 2σ confidence level.

4. Discussion

We have observed A2218 with the XIS instrument onboard *Suzaku* to search for the redshifted O emission lines from the WHIM, which is possibly forming a large-scale filament around the cluster. The object was selected because its redshift ($z = 0.1756$) would allow the XIS to separate the WHIM lines from the Galactic ($z = 0$) ones, and because an elongated structure in the line-of-sight direction was suggested from the previous studies of this cluster. We detected no redshifted O lines, and set a constraint on their intensities. In this section, we compare our constraints on the line intensity with those reported in other works and also discuss the future prospect of studying the WHIM emission with the *Suzaku* XIS.

4.1. Comparison with other results

Kaastra et al. (2003) and Finoguenov et al. (2003) reported positive detections of O lines around clusters of galaxies based on *XMM-Newton* observations. Kaastra et al. (2003) detected significant O lines in three clusters, Sérsic 159–03, MKW 3s and A2052, and possible, but not uniquely proven, O lines in the Coma and A1795 clusters. Finoguenov et al. (2003) detected the O lines in the outskirts of the Coma cluster, in particular, the Coma-11 field. Fig. 7 compares the O line surface brightness I for their observations and our results. The left and right panels are for the O VII and O VIII cases, respectively. The intensity of the O lines of Galactic emission measured by a microcalorimeter experiment of McCammon et al. (2002), the one compiled by Lumb et al. (2002) and the one estimated from our Offset-A observation are also shown. The surface brightness quoted for Kaastra et al. (2003) was calculated using the temperature and emission measure in their Table 7 and the metal abundance from Tables 4 and 5 of Tamura et al. (2004), assuming the solar abundance ratio Fe to O (Fe/O number density ratio of 0.55; Anders & Grevesse, 1989). The surface brightness levels of the O VII or O VIII emission lines that were reported so far from the *XMM-Newton* observations are similar to or higher than that of the Galactic emission. In contrast, the upper limit of O VII line intensity in the A2218 vicinity obtained in this work is about six times lower than the Galactic level. The upper limit for O VIII is also lower than the level reported as a positive detection in other works. The tight upper limit we obtained here demonstrates the good spectral capability of the XIS, in particular below 0.5 keV.

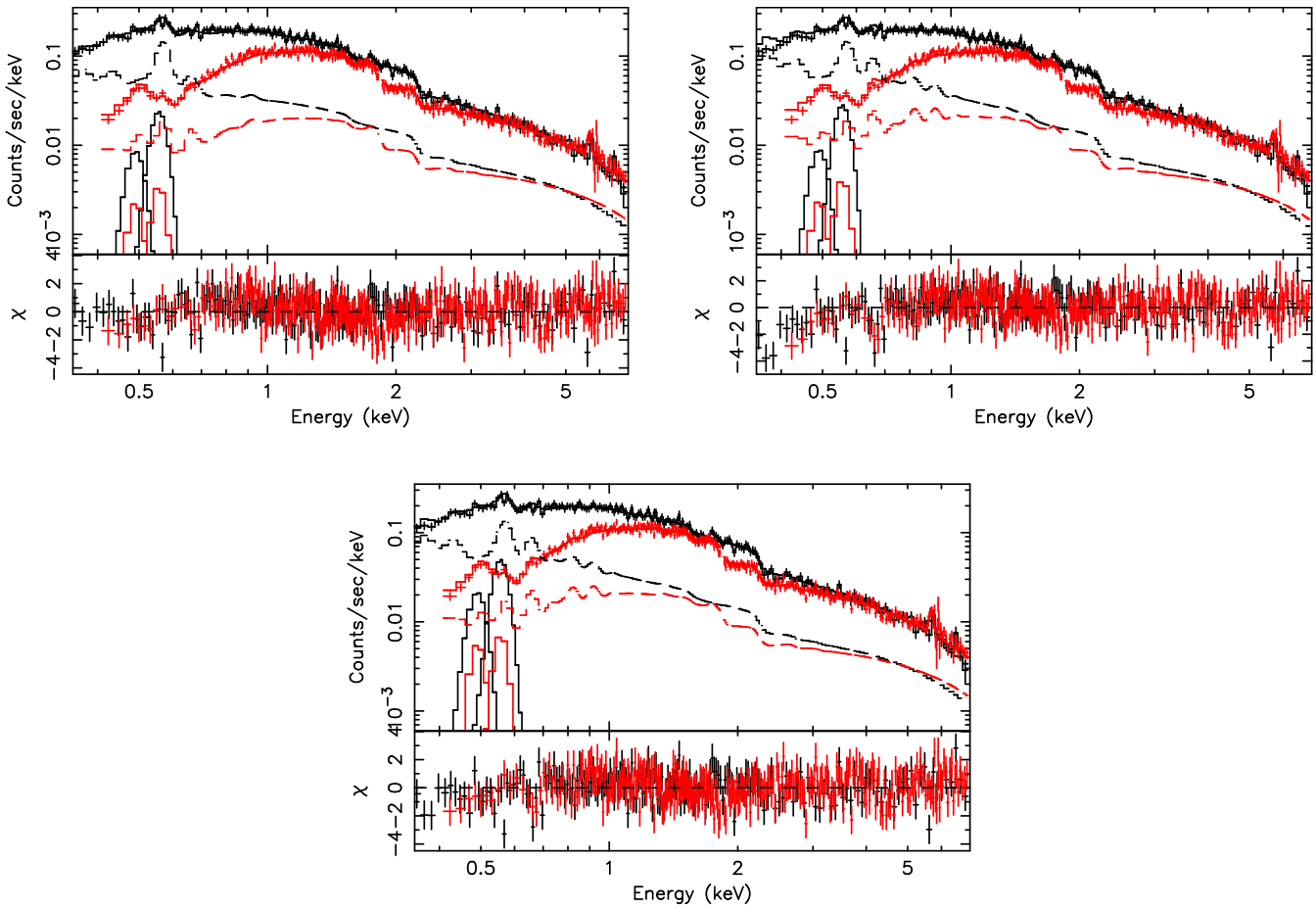

Fig. 6. A2218 BI (black) and FI (red) spectra and models with redshifted O lines. The two emission lines indicated with solid lines in the 0.4–0.6 keV range show the maximum allowed level (2σ) of O VII and O VIII lines. Dashed lines indicate the background emission. (upper left) without considering systematic uncertainty, using the best-fit model of Offset-A observation as the Galactic emission. (upper right) without considering systematic uncertainty, using Offset-B observation. (bottom) the model of maximum O line intensity after considering systematic uncertainties: with ARFs of 20% thicker contaminant and 10% fainter Galactic model than the one determined from the Offset-B observation. The O VII and O VIII surface brightness was $1.1 \times 10^{-7}$and 2.7×10^{-7} photons cm^{-2} s^{-1} arcmin^{-2}, respectively.

4.2. Constraint on the WHIM density

If we assume that the O VII emission line is produced in a cloud with uniform density and temperature under collisional ionization equilibrium, the surface brightness I is determined by the electron density $n_{\rm e}$, the hydrogen density $n_{\rm H}$, path length L, and metal abundance Z of the cloud as

$$I = C(T)\ (1+z)^{-3}\ n_{\rm e} n_{\rm H}\ ZL, \tag{1}$$

where $C(T)$ is a coefficient that depends on the temperature of the cloud. Here, we will constrain the density of the cloud assuming the temperature to be $T \sim 2 \times 10^6$ K, since the O VII line is strongest at this temperature. Substituting $C(T = 2 \times 10^6\ {\rm K})$ with the value calculated with the SPEX code (Kaastra et al., 1996), our constraint, $I < 1.1 \times 10^{-7}$ photons cm^{-2} s^{-1} arcmin^{-2} at $z = 0.1756$, and electron-to-hydrogen number density ratio $n_{\rm e}/n_{\rm H} = 1.2$ for ionized gas, gives the following condition

$$n_{\rm H} < 7.8 \times 10^{-5}\ {\rm cm}^{-3} \left(\frac{Z}{0.1\ Z_\odot}\right)^{-1/2} \left(\frac{L}{2\ {\rm Mpc}}\right)^{-1/2}. \tag{2}$$

Note that $L = 2$ Mpc corresponds to $11'$, the average diameter of the annular region where we extracted the spectra. The overdensity $\delta \equiv n_{\rm H}/\bar{n}_{\rm H}$ of this cloud is

$$\delta < 270 \left(\frac{Z}{0.1\ Z_\odot}\right)^{-1/2} \left(\frac{L}{2\ {\rm Mpc}}\right)^{-1/2}, \tag{3}$$

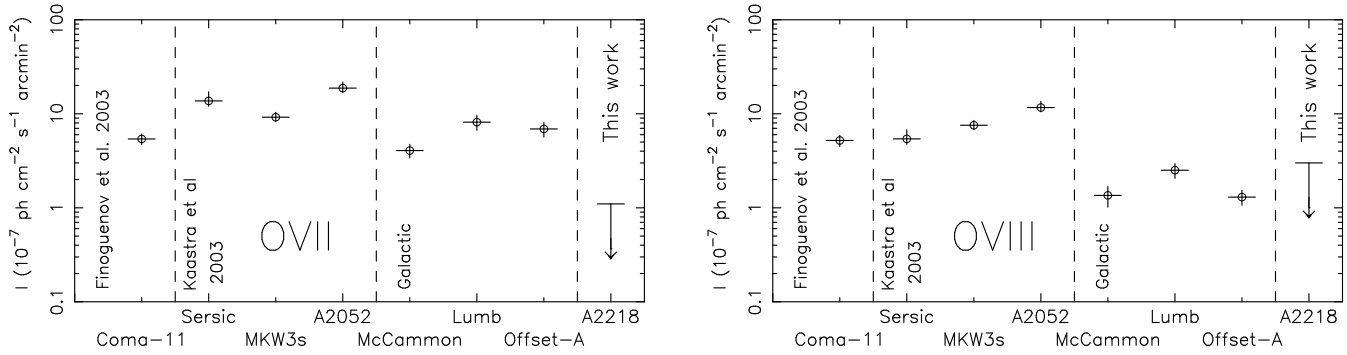

Fig. 7. Comparison of O VII (left) and O VIII (right) surface brightness. From left to right, those in the Coma-11 field (Finoguenov et al., 2003), Sérsic 159–03, MKW 3s and A2052 (Kaastra et al., 2003), Galactic emission of McCammon et al. (2002), Lumb et al. (2002), and our Offset-A observation, and the upper limits in A2218 outskirts (this work) are plotted.

where $\bar{n}_{\rm H} = X\Omega_{\rm b}\rho_{\rm crit}(1+z)^3/m_{\rm p} = 1.77\times10^{-7}\ (1+z)^3\ {\rm cm}^{-3}$ is the mean hydrogen density in the universe, in which $X = 0.71$ is the hydrogen-to-baryon mass ratio, $\Omega_{\rm b} = 0.0457$ is the baryon density of the universe, $\rho_{\rm crit} = 9.21\times10^{-30}$ g cm^{-3} is the critical density of the universe, and $m_{\rm p}$ is the proton mass. Even though this level of overdensity is much higher than the typical WHIM density ($\delta \sim 10$), it shows that Suzaku can certainly detect the high-density end of the WHIM distribution that is predicted to exist near clusters.

4.3. Prospect for the WHIM observation with the XIS

Although we have set a tight constraint on the intensity of redshifted O lines, the inherent sensitivity of the XIS was presumably not achieved, since the redshifted O VIII line fell almost on the Galactic O VII line, while the redshifted O VII line overlapped with the instrumental neutral O edge. Therefore, better sensitivity is expected for clusters with a redshift such that the redshifted lines are free from the Galactic and instrumental features. For example, a redshift of $z \sim 0.07$ or $z > 0.2$ is suitable for this purpose. The former case is more promising, because the surface brightness of high-z clusters is lower and because the contamination of bright ICM emission in the center of the cluster makes the detection of warm-hot emission in the outskirts difficult for distant clusters. Note that the XIS is capable of separating a redshift difference of $\Delta z \sim 0.07$ at the O line energy.

Because of the contamination on the XIS OBF, the effective area at the redshifted O VII line had dropped by $\sim 25\%$ at the time of the A2218 observation. If there had been no contamination on the OBF, we could have obtained more photons by this fraction. This contamination also caused a large systematic uncertainty corresponding to about 5% of the OVII line flux. Since the thickness and chemical composition of the contaminant will be better understood as more data are accumulated, the uncertainty will be less influential in future observations. Furthermore, we hope that the original XIS sensitivity in the soft X-ray energy range can be recovered in the future by hardware changes including warming the contaminated OBFs.

It should be noted that in most cases concerning the search for faint WHIM emission with CCD sensors, the variation of Galactic emission causes a larger uncertainty than the statistical one. Offset observations, such as those carried out in our work, are always desirable to determine the background emission level reliably. Looking at a somewhat longer time frame, observations with microcalorimeters are promising, because their outstanding energy resolution ($\Delta E \lesssim 7$ eV) for extended sources can easily separate the WHIM emission from the Galactic spectral features. For example, two orders of magnitude higher sensitivity than the present work is expected with a small mission such as *DIOS* (Diffuse Ionized Oxygen Surveyor; Ohashi et al., 2006), which is proposed to be launched in early 2010s (Yoshikawa et al., 2004).

5. Summary

We used *Suzaku* XIS observations to constrain the intensity of O emission lines around the cluster of galaxies A2218. After considering systematic uncertainties mainly caused by the Galactic emission and the uncertainty in the detector response, we obtained upper limits for the surface brightness of the O VII and O VIII lines of 1.1×10^{-7} photons cm^{-2} s^{-1} arcmin^{-2} and 3.0×10^{-7} photons cm^{-2} s^{-1} arcmin^{-2}, respectively. These upper limits are significantly lower than the previously reported fluxes around other clusters of galaxies. Our tight constraints demonstrate the sensitivity of the XIS for redshifted O lines.

We are grateful to Dr. S. Sasaki for valuable comments on cosmological parameters and the anonymous referee for important comments. YT would like to thank Prof. D. McCammon for a lot of information and comments regarding

the Galactic emission, and Dr. N. White for careful internal review of the manuscript. The authors would like to thank ISAS/JAXA and the entire *Suzaku* team for the opportunity to participate in the development of the *Suzaku* mission as members of its Science Working Group. YT is supported by grants from the JSPS Research Fellowship for Young Scientists (DC 16-10681 and PD 18-7728). This work is supported by Grant-in-Aid for Science Research of JSPS and MEXT (KAKENHI 14079103, 15340088 and 16002004), and NASA grant (NNG05GP87G, NNG05GM92G, NNG06GC04G).

References

Anders, E., & Grevesse, N. 1989, Geochimica et Cosmochimica Acta, 53, 197
Bonamente, M., Lieu, R., & Kaastra, J. 2005, A&A, 443, 29
Bowyer, S., Korpela, E. J., Lampton, M., & Jones, T. W. 2004, ApJ, 605, 168
Bregman, J. N., & Lloyd-Davies, E. J. 2006, ApJ, 644, 167
Cen, R., & Ostriker, J. P. 1999, ApJ, 514, 1
Chen, X., Weinberg, D. H., Katz, N., & Davé, R. 2003, ApJ, 594, 42
Danforth, C. W., & Shull, J. M. 2005, ApJ, 624, 555
Davé, R., et al. 2001, ApJ, 552, 473
Dickey, J. M., & Lockman, F. J. 1990, ARAA, 28, 215
Finoguenov, A., Briel, U. G., & Henry, J. P. 2003, A&A, 410, 777
Fujimoto, R., et al. 2004, PASJ, 56, L29
Fukugita, M., Hogan, C. J., & Peebles, P. J. E. 1998, ApJ, 503, 518
Girardi, M., Fadda, D., Escalera, E., Giuricin, G., Mardirossian, F., & Mezzetti, M. 1997, ApJ, 490, 56
Ishisaki, Y., et al. 2006, PASJ, this volume, submitted
Kaastra, J. S., Mewe, R., & Nieuwenhuijzen, H. 1996, in UV and X-ray Spectroscopy of Astrophysical and Laboratory Plasma, ed. K. Yamashita & T. Watanabe (Tokyo : Universal Academy) 411
Kaastra, J. S., Lieu, R., Tamura, T., Paerels, F. B. S., & den Herder, J. W. 2003, A&A, 397, 445
Kaastra, J. S. 2004, Journal of Korean Astronomical Society, 37, 375
Kaastra, J. S., Werner, N., den Herder, J. W. A., Paerels, F. B. S., de Plaa, J., Rasmussen, A. P., & de Vries, C. P. 2006, ApJ submitted, `astro-ph/0604519`
Koyama, K., et al. 2006, PASJ, this volume, submitted
Kushino, A., Ishisaki, Y., Morita, U., Yamasaki, N. Y., Ishida, M., Ohashi, T., & Ueda, Y. 2002, PASJ, 54, 327
Lieu, R., Mittaz, J. P. D., Bowyer, S., Breen, J. O., Lockman, F. J., Murphy, E. M., & Hwang, C.-Y. 1996a, Science, 274, 1335
Lieu, R., Mittaz, J. P. D., Bowyer, S., Lockman, F. J., Hwang, C.-Y., & Schmitt, J. H. M. M. 1996b, ApJL, 458, L5+
Lumb, D. H., Warwick, R. S., Page, M., & De Luca, A. 2002, A&A, 389, 93
Machacek, M. E., Bautz, M. W., Canizares, C., & Garmire, G. P. 2002, ApJ, 567, 188
McCammon, D., Almy, R., Apodaca, E., Bergmann Tiest, W., Cui, W., Deiker, S., Galeazzi, M., Juda, M., Lesser, A., Mihara, T., Morgenthaler, J. P., Sanders, W. T., Zhang, J., Figueroa-Feliciano, E., Kelley, R. L., Moseley, S. H., Mushotzky, R. F., Porter, F. S., Stahle, C. K., & Szymkowiak, A. E. 2002, ApJ, 576, 188
Mitsuda, K., et al. 2006, PASJ, this volume, submitted
Mittaz, J. P. D., Lieu, R., & Lockman, F. J. 1998, ApJL, 498, L17+
Nicastro, F., et al. 2005, ApJ, 629, 700
Ohashi, T., et al. 2006, in SPIE proceedings of "Astronomical Telescopes and Instrumentation", Vol. 6266, in press
Pratt, G. W., Böhringer, H., & Finoguenov, A. 2005, A&A, 433, 777
Rauch, M., et al. 1997, ApJ, 489, 7
Rasmussen, A. P., Kahn, S. M., Paerels, F., Willem den Herder, J., Kaastra, J., & de Vries, C. 2006, ApJ submitted, `astro-ph/0604515`
Smith, G. P., Kneib, J.-P., Smail, I., Mazzotta, P., Ebeling, H., & Czoske, O. 2005, MNRAS, 359, 417
Snowden, S. L., et al 1997, ApJ, 485, 125
Snowden, S. L., Egger, R., Finkbeiner, D. P., Freyberg, M. J., & Plucinsky, P. P. 1998, ApJ, 493, 715
Spergel, D. N., et al. 2003, ApJS, 148, 175
Struble, M. F., & Rood, H. J. 1999, ApJS, 125, 35
Takei, Y., Henry, J. P., Finoguenov, A., Mitsuda, K., Tamura, T., Fujimoto, R., & Briel, U. G. 2006, ApJ, submitted
Tamura, T., Kaastra, J. S., den Herder, J. W. A., Bleeker, J. A. M., & Peterson, J. R. 2004, A&A, 420, 135
Yoshikawa, K., et al. 2004, PASJ, 56, 939